High-Performance Computing in Biomedical Research

Edited by
Theo C. Pilkington
Bruce Loftis
Joe F. Thompson
Savio L-Y. Woo
Thomas C. Palmer
Thomas F. Budinger

CRC Press
Boca Raton Ann Arbor London Tokyo

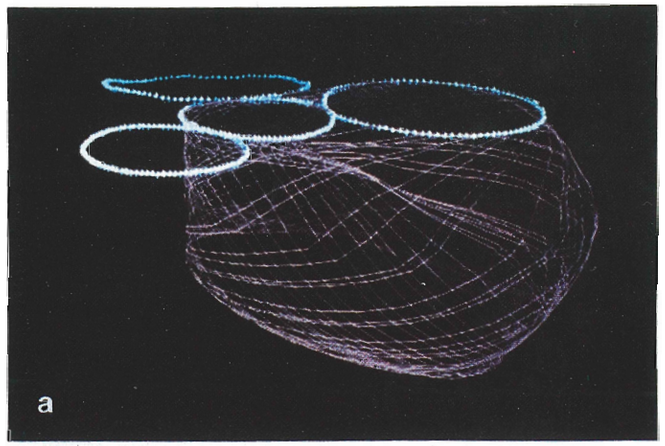

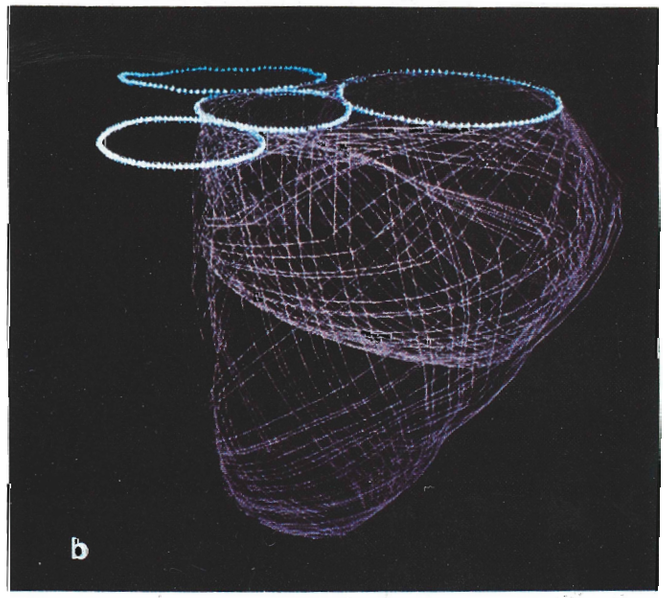

PLATE 6. Anatomy of the three-dimensional model heart. The model heart is composed of several layers, each constructed by laying fibers along geodesic paths on selected surfaces in three-space. The path of every fiber of the heart wall lies partially on the valve rings, which are shown in white. (a) The smallest of the intramural layers of the left ventricle. Here the surfaces on which fibers lie are essentially two truncated cones with a common edge curve at the bottom and an annular separation at the level of the equator. Fibers spiraling upward on both sides of this annulus are drawn together onto the mitral valve ring by means of interpolating surfaces. (b) Two of the intramural layers of the left ventricle. The smaller of these two layers (also shown in Plate 6a) is completely contained within the surfaces of the larger layer. (c) All four of the intramural layers of the left ventricle. In the real heart there is a continuum of such layers. (d) The mitral valve (leaflets, chordae tendinae, and papillary muscles) and the aortic valve leaflets. (e) The valves of Plate 6d, the intramural layers of Plate 6c, and the aorta. (f) All four valves, the aorta, the pulmonary artery, and both ventricles. The right ventricle consists of fibers lying primarily on a conical surface of crescent-shaped cross section, partially wrapped around the left ventricle. The outermost layer of the heart is primarily a conical surface whose fibers are rays of the cone. The tips of the right ventricular cone and the outermost cone are at the apex of the heart. (g) The entire three-dimensional model heart. (h) The entire three-dimensional model heart with a portion of the fibers nearest the viewer clipped away to permit a view into the interior.

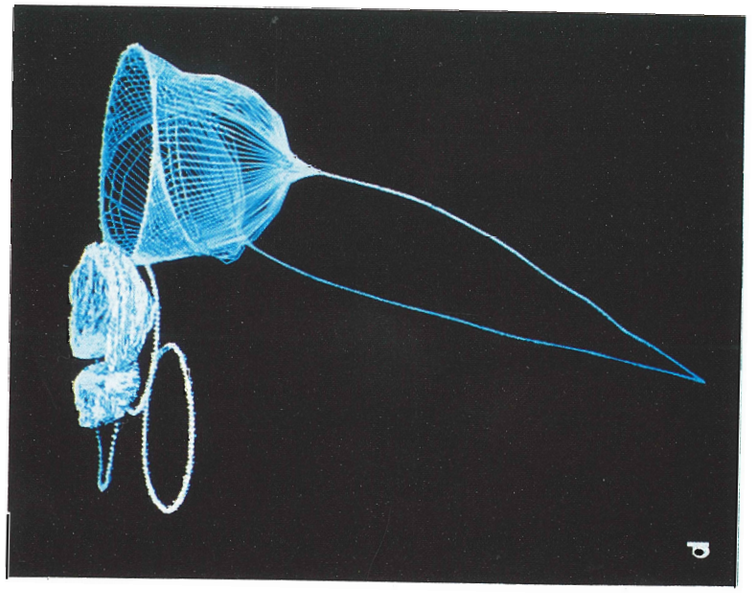

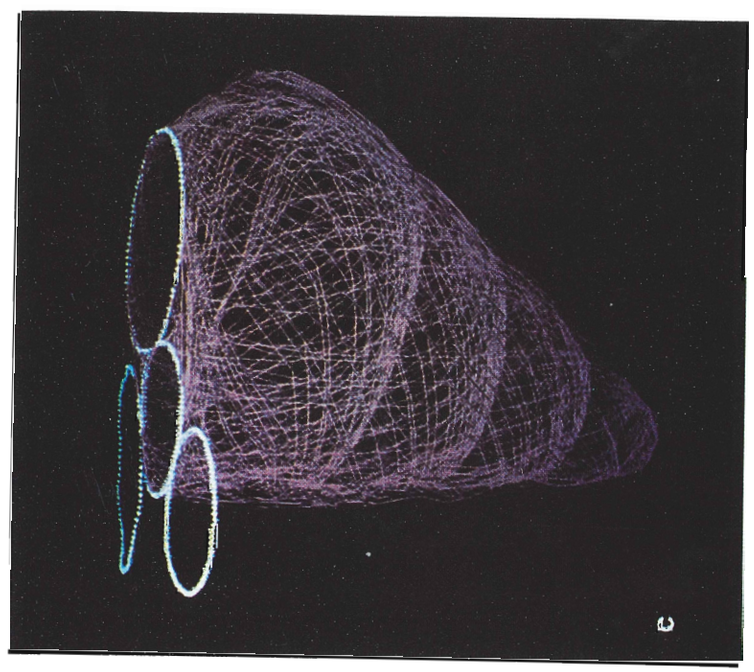

PLATE 6 *(continued)*

PLATE 6 *(continued)*

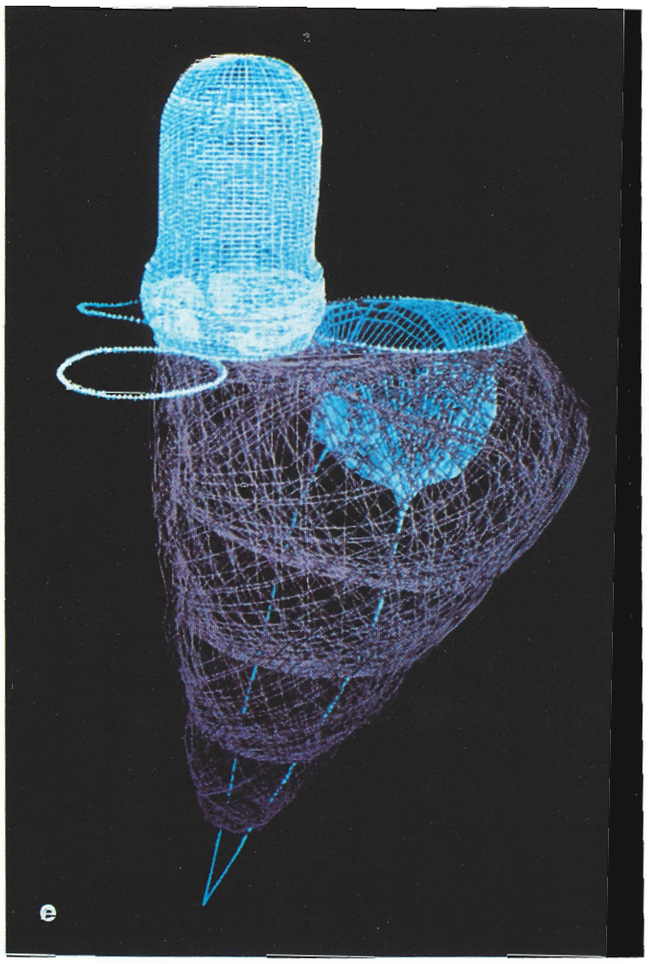

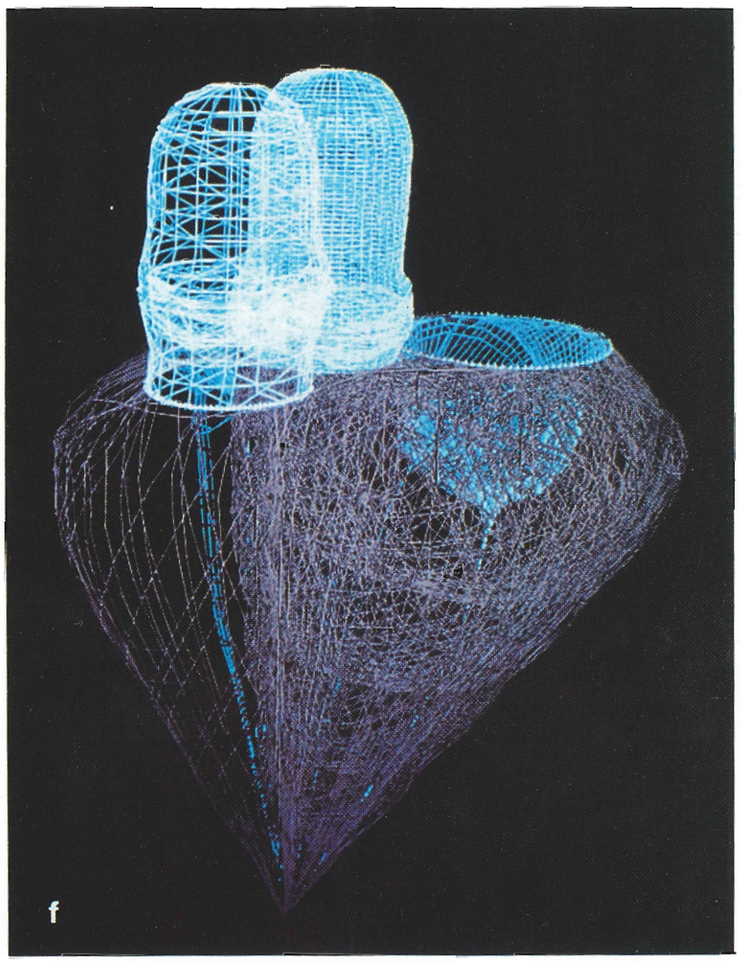

PLATE 6 *(continued)*

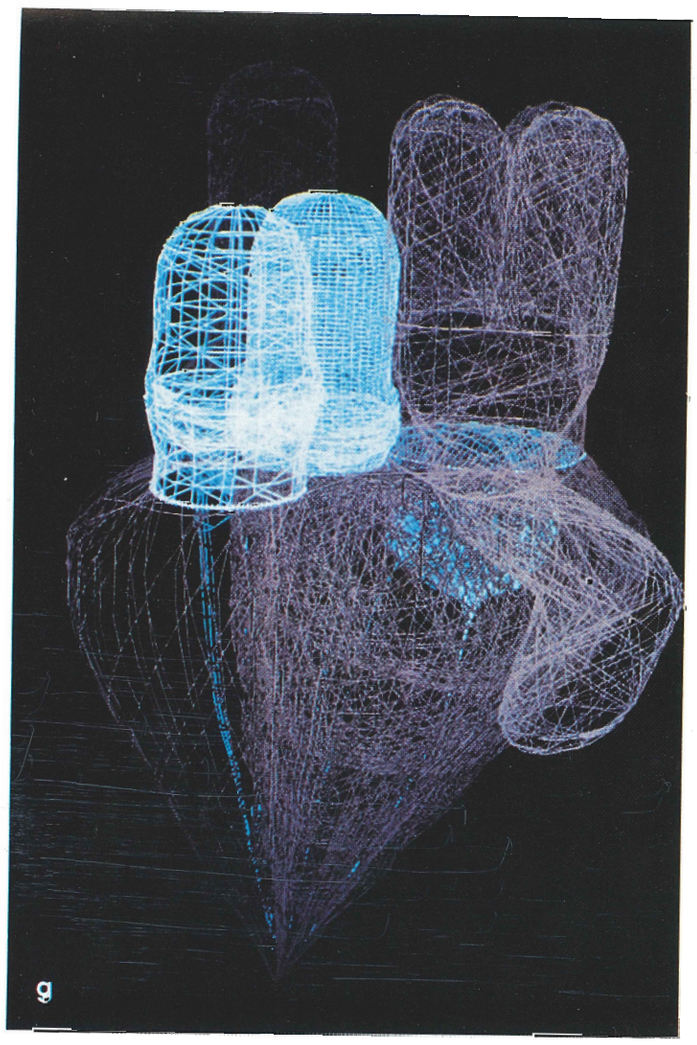

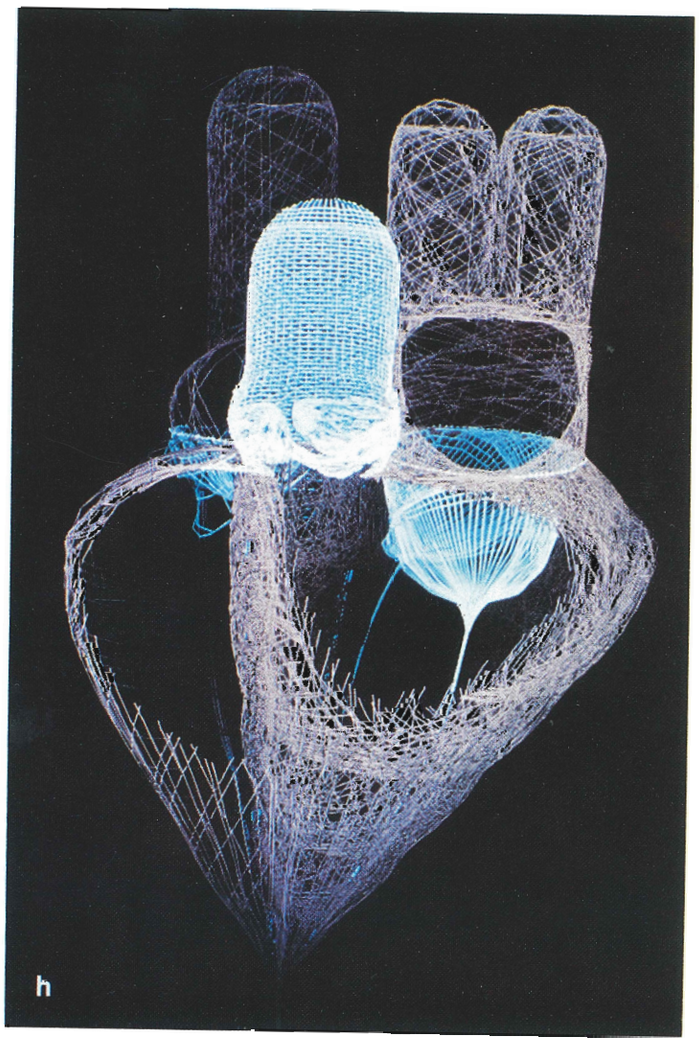

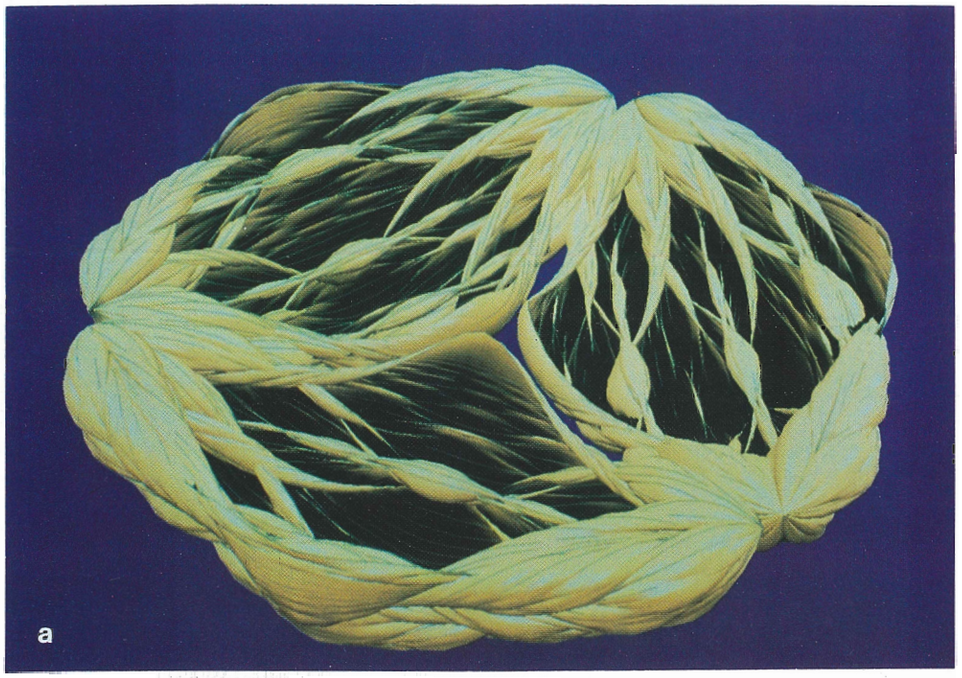

PLATE 7. Fiber architecture of the aortic valve. (a) Computer-generated image showing the three leaflets of the model aortic valve in its closed position. The fiber architecture of the valve has a fractal structure that has here been predicted by solving a partial differential equation for the mechanical equilibrium of the fibers under a pressure load. In this figure, the leaflets have been rendered as surfaces; the grayish lines that can be seen running along the surfaces are a subset (1 out of every 16) of the computed fibers. (b) The same view as in Plate 7a, but the surface is not rendered: only the fibers (one out of every four) are shown. (c) One leaflet of the real aortic valve, stained for collagen and mounted on a flat surface. The small round holes around the border are artifacts of the mounting process. The free leaflet margins are the two curves at the top. The point at the top of the figure where the free margins meet is the center of the valve, where all three leaflets come together during valve closure. The remainder of the leaflet boundary (other than the free margins) is attached to the wall of the aorta. The extreme left and right ends of the attached boundary (where it meets the free margins) are the two commisural points of the leaflet. Note how most of the collagen fibers radiate out from these commisural points in thick cables, which later branch to cover the surface of the leaflet. These cables form ridges on the concave side of the leaflet surface, as predicted by the theory. (Plate 7c is reproduced by permission from the Ph.D. thesis of Sauren,[21] page 14.)

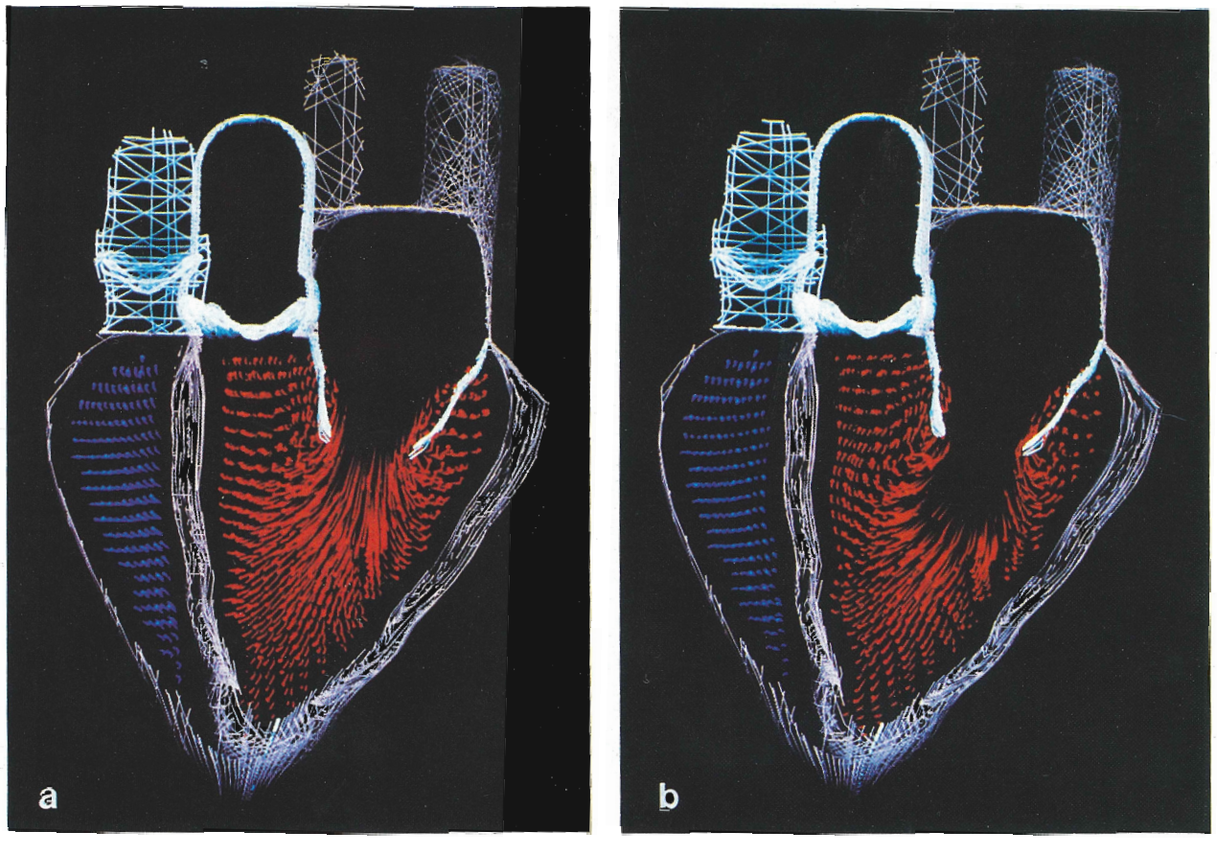

PLATE 8. Computed flow patterns in a thin slice of the three-dimensional heart model at different times during a single heartbeat. The slice is fixed in space, whereas the heart is free to move. The slice passes through the mitral and aortic valves, between the pulmonic and tricuspid valves (which are consequently not visible), and near the apex. The light reddish brown lines are segments of muscle fibers, the white lines are segments of the valve leaflet or artery fibers, and the red and blue streaks indicate the recent motion of left and right ventricular blood, respectively. (a and b) Flow patterns at two instants of time near the peak of early diastolic filling. (c and d) Flow patterns at two instants of time just after the onset of ventricular ejection. Because of the position of the slice between the right ventricular valves, relatively little motion of right ventricular blood is visible.

PLATE 8 *(continued)*

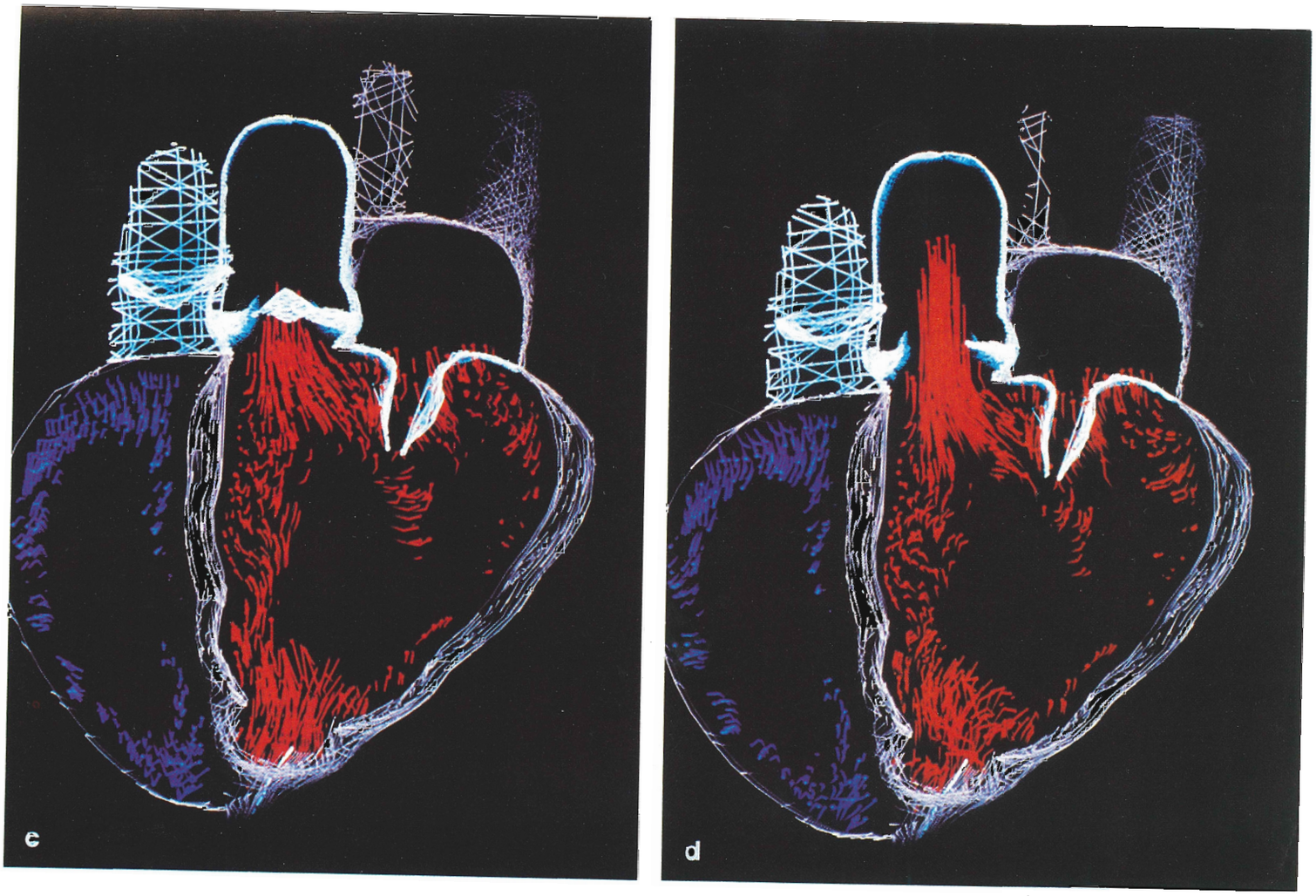

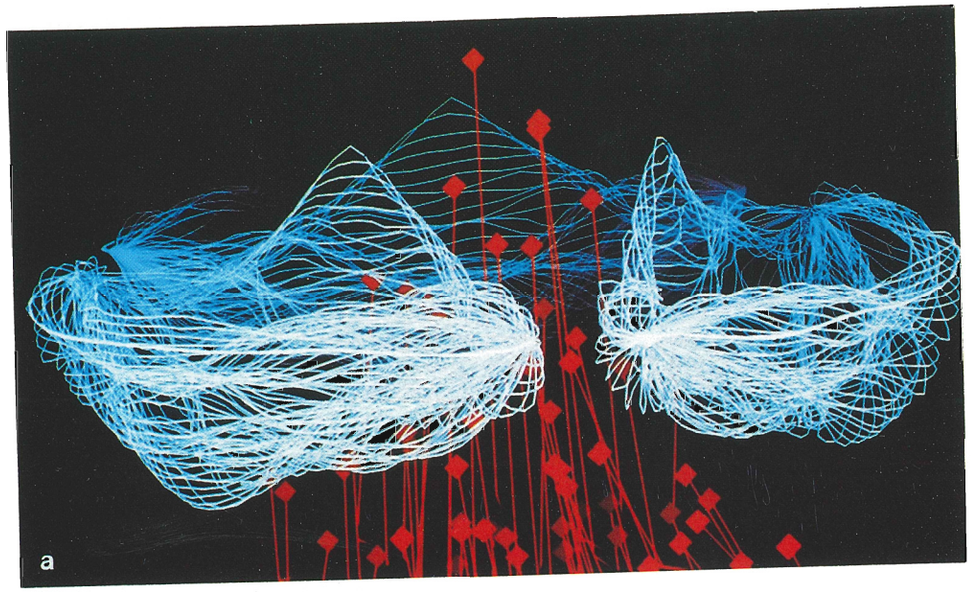

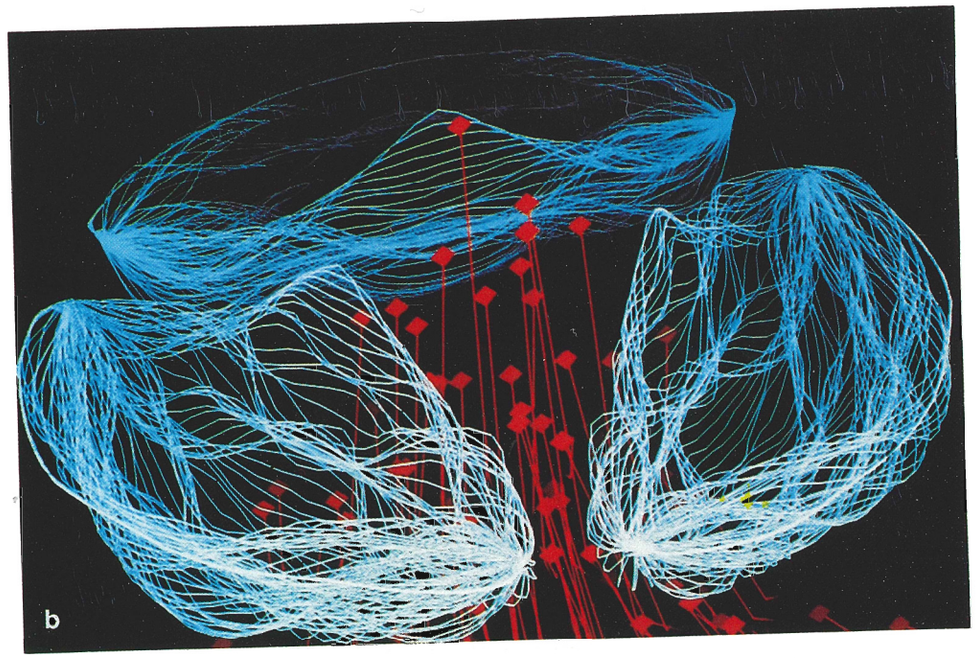

PLATE 9. Two views of flow in the neighborhood of the aortic valve early in ventricular ejection (see Plate 8c). The valve leaflet fibers are shown in white, the red blobs are left ventricular blood markers, and the red streaks mark the recent paths of the blobs. (a) A view from above, looking down from a relatively small angle of inclination to the "plane" of the aortic valve ring. (b) A view from above, looking down from a somewhat larger angle of inclination.

Chapter 3

CARDIAC FLUID DYNAMICS

Charles S. Peskin and David M. McQueen

TABLE OF CONTENTS

I. Introduction: The Equations of Cardiac Fluid Dynamics 52

II. Computational Method 53

III. Three-Dimensional Model: Results 56

IV. Summary and Conclusions 58

Acknowledgments 58

References 58

ISBN 0-8493-4474-3

ABSTRACT

The heart is modeled as a system of elastic and/or contractile fibers immersed in a viscous incompressible fluid. Simulated heart walls and valves are constructed by arranging the fibers according to an idealized version of the actual distribution of muscle fibers in the heart walls and collagen fibers in the valve leaflets. Then the combined motion of the fluid–fiber system is predicted through the numerical solution of its coupled equations of motion. Fluid equations are solved by a finite difference method on a fixed, regular computational lattice. Fiber points move freely through this lattice without being constrained to lie at the lattice intersections. Communication between fibers and fluid involves interpolation of the fluid velocity to the fiber points and the spreading of the fiber forces to the computational lattice of the fluid. Both of these operations make use of a smoothed approximation to the Dirac delta function. The entire method is suitable for implementation on vector, parallel, or parallel-vector hardware. Applications include the investigation of normal cardiac function, the simulation of disease processes affecting the mechanical function of the heart or its valves, and the computer-assisted design of prosthetic cardiac valves.

I. INTRODUCTION: THE EQUATIONS OF CARDIAC FLUID DYNAMICS

The dynamics of blood flow in the cardiac chambers cannot be separated from the mechanics of the elastic and contractile tissues of the heart itself. These tissues are fiber-reinforced, the fibers in question being primarily muscle fibers in the case of the heart walls and primarily collagen fibers in the case of the heart valve leaflets. The entire system, comprised of muscle, blood, and valves, is effectively incompressible and has an essentially constant density ρ.

The external tissue surrounding the heart also has some influence on the cardiac mechanics. We model this influence in a simple way, by treating the heart as though it were immersed in a fluid with the same density and viscosity as blood.

From these considerations, we are led to consider the problem of a viscous incompressible fluid containing an immersed system of elastic or contractile fibers. (A fiber is "contractile" if its elastic parameters, such as stiffness or rest length, are time-dependent.) The fibers themselves are regarded as massless force-generating elements. Together with the fluid in which they are immersed, they model a composite material, for which we may write the equations of motion:

$$\rho\left(\frac{\partial \mathbf{u}}{\partial t} + \mathbf{u}\cdot\nabla\mathbf{u}\right) + \nabla p = \mu\nabla^2\mathbf{u} + \mathbf{F}, \tag{1}$$

$$\nabla\cdot\mathbf{u} = 0, \tag{2}$$

$$\mathbf{F}(\mathbf{x},t) = \int \mathbf{f}(q,r,s,t)\,\delta^3(\mathbf{x} - \mathbf{X}(q,r,s,t))\,dq\,dr\,ds, \tag{3}$$

$$\frac{\partial \mathbf{X}}{\partial t}(q,r,s,t) = \mathbf{u}(\mathbf{X}(q,r,s,t),t) \tag{4a}$$

$$= \int \mathbf{u}(\mathbf{x},t)\,\delta^3(\mathbf{x} - \mathbf{X}(q,r,s,t))\,d^3\mathbf{x}, \tag{4b}$$

$$\mathbf{f} = \frac{\partial}{\partial s}(T\boldsymbol{\tau}), \tag{5}$$

$$T = \sigma\left(\left|\frac{\partial \mathbf{X}}{\partial s}\right|; q, r, s, t\right), \tag{6}$$

$$\boldsymbol{\tau} = \frac{\partial \mathbf{X}/\partial s}{|\partial \mathbf{X}/\partial s|}. \tag{7}$$

These equations are based on a mixed Eulerian–Lagrangian description of the motion. The Eulerian variables are the velocity $\mathbf{u}(\mathbf{x}, t)$, the pressure $p(\mathbf{x}, t)$, and the force $\mathbf{F}(\mathbf{x}, t)\, d^3\mathbf{x}$ which is applied by the fibers to the fluid in which they are immersed. Here $\mathbf{x}$ denotes position in space, $d^3\mathbf{x}$ is the volume element, and t is the time. The Lagrangian variables are the fiber point position $\mathbf{X}(q, r, s, t)$, the fiber tension $T(q, r, s, t)\, dq\, dr$, the unit tangent to the fibers $\boldsymbol{\tau}(q, r, s, t)$, and the resultant fiber force $\mathbf{f}(q, r, s, t)\, dq\, dr\, ds$. (Note that $\mathbf{f}$ and $\mathbf{F}$ are corresponding force densities.) Here q, r, and s are curvilinear coordinates chosen in such a way that (q, r) labels a particular fiber and (q, r, s) labels a particular material point. As written here, the equations describe a three-dimensional system of fibers, as is appropriate for the thick heart wall. The modification required for the description of a fiber-reinforced surface such as a valve leaflet is simply to drop one of the indices q or r. In that case Equation 3 involves only a double integration, but it still contains a three-dimensional delta function. The result is a singular force field in which the force density $\mathbf{F}$ is infinite on the surface in question but has a finite integral over any definite volume.

Note that Equations 1–7 may be divided into three groups. Equations 1 and 2, in which the independent variables are $(\mathbf{x}, t)$, are the Navier–Stokes equations for a viscous incompressible fluid of density ρ and viscosity μ moving under the influence of an applied force density $\mathbf{F}$. Here, however, the force density is not externally applied, but arises from the fibers that are immersed in the fluid. Equations 5–7, in which the independent variables are (q, r, s, t), are the fiber equations that may be used to determine the Lagrangian fiber force density $\mathbf{f}$ from the fiber configuration $\mathbf{X}$ at time t. In Equation 6, $|\partial \mathbf{X}/\partial s|$ determines the fiber strain, and the function σ defines the (possibly nonlinear) stress–strain relation of the fibers. Note in particular the explicit time-dependence in σ that allows the heart to contract and relax. Equations 3 and 4 are the interaction equations that connect the functions of $(\mathbf{x}, t)$ and the functions of (q, r, s, t). Both involve integral transformation in which the Dirac delta function appears as a kernel. (The notation δ^3 denotes the three-dimensional delta function, which may be expressed as a product of three one-dimensional delta functions.) Note that Equation 4 is the familiar no-slip condition, which here plays the unfamiliar role of an equation of motion for the fibers, because the fiber motion is not specified in advance. For various derivations and for further discussion of Equations 1–7, see References 1–5.

II. COMPUTATIONAL METHOD

Equations 1–7 are solved by the immersed boundary method,[1–5] which will be briefly summarized here. In this method, the Eulerian (fluid) variables are defined on a fixed cubic computational lattice, the structure of which is not altered or interrupted in any way by the presence of the fibers. Lagrangian variables are defined on discrete computational fibers, each of which is a list of discrete fiber points that are thought of

as being connected by (possibly nonlinear) springs, the elastic parameters of which may be time-dependent. The fibers move freely through the computational lattice of the fluid: there is no requirement that the fiber points and the lattice points should coincide.

At the beginning of each time step, the fluid velocity **u** and the fiber configuration **X** are given. These quantities are updated as follows:

1. Use the fiber configuration **X** to determine the Lagrangian density **f** of the fiber force. This is done by straightforward application of Equations 5–7 in finite-difference form. Only the fiber data are involved.
2. Determine the Eulerian force density **F** from the Lagrangian force density **f**. This step is based on a discretization of Equation 3, as described in succeeding text.
3. Update the fluid velocity **u** under the influence of the applied force density **F**. This requires the numerical integration of the Navier–Stokes equations (Equations 1 and 2), which is done by the projection method.[6,7] Only the Eulerian (fluid) data are involved.
4. Interpolate the fluid velocity at the fiber points and update the fiber configuration **X**. This step is based on a discretization of Equation 4b, as described in succeeding text.

Because the fluid velocity and the fiber configuration both have been updated, this completes the time step.

In the algorithm that we have just described, Steps 2 and 4 are based on a discretization of the interaction equations, Equations 3 and 4b. In this discretization, the integrals are replaced by sums and the Dirac delta function δ^3 is replaced by an approximate delta function δ_h^3, which is a product of three one-dimensional functions of the form

$$\delta_h(x) = \frac{1}{4h}\left(1 + \cos\left(\frac{\pi x}{2h}\right)\right), \qquad |x| < 2h, \tag{8}$$

with $\delta_h(x) = 0$, otherwise. (In this formula, h is the mesh width of the computational lattice on which the fluid variables are defined.) The motivation for this particular choice of δ_h is discussed in References 1 and 2.

The virtue of this numerical method is that the fixed regular structure of the fluid dynamics computation is not altered in any way by the complicated, time-dependent, and unknown geometry of the heart and its valves. Indeed, the cardiac fibers only make themselves felt in the fluid dynamics computation through the Eulerian force density **F**, which is defined on the computational lattice of the fluid.

We conclude this section with a mathematical statement of the immersed boundary method. The equations are grouped according to the steps of the algorithm as previously described.

Step 1:

$$T^n = \sigma\left(|D_s^+ \mathbf{X}^n|; q, r, s + \frac{\Delta s}{2}, n\,\Delta t\right), \tag{9}$$

$$\boldsymbol{\tau}^n = \frac{D_s^+ \mathbf{X}^n}{|D_s^+ \mathbf{X}^n|}, \tag{10}$$

$$\mathbf{f}^n = D_s^-(T^n \boldsymbol{\tau}^n). \tag{11}$$

Step 2:

$$\mathbf{F}^n(\mathbf{x}) = \sum_{q,r,s} \mathbf{f}^n(q,r,s)\,\delta_h^3(\mathbf{x} - \mathbf{X}^n(q,r,s))\,\Delta q\,\Delta r\,\Delta s. \tag{12}$$

Step 3:

$$\rho \frac{\mathbf{u}^{n+1,0} - \mathbf{u}^n}{\Delta t} = \mathbf{F}^n, \tag{13}$$

$$\rho\left(\frac{\mathbf{u}^{n+1,1} - \mathbf{u}^{n+1,0}}{\Delta t} + u_1^n D_{x_1}^0 \mathbf{u}^{n+1,1}\right) = \mu D_{x_1}^+ D_{x_1}^- \mathbf{u}^{n+1,1}, \tag{14}$$

$$\rho\left(\frac{\mathbf{u}^{n+1,2} - \mathbf{u}^{n+1,1}}{\Delta t} + u_2^n D_{x_2}^0 \mathbf{u}^{n+1,2}\right) = \mu D_{x_2}^+ D_{x_2}^- \mathbf{u}^{n+1,2}, \tag{15}$$

$$\rho\left(\frac{\mathbf{u}^{n+1,3} - \mathbf{u}^{n+1,2}}{\Delta t} + u_3^n D_{x_3}^0 \mathbf{u}^{n+1,3}\right) = \mu D_{x_3}^+ D_{x_3}^- \mathbf{u}^{n+1,3}, \tag{16}$$

$$\rho \frac{\mathbf{u}^{n+1} - \mathbf{u}^{n+1,3}}{\Delta t} + \mathbf{D}^0 p^{n+1} = 0, \tag{17}$$

$$\mathbf{D}^0 \cdot \mathbf{u}^{n+1} = 0. \tag{18}$$

Step 4:

$$\frac{\mathbf{X}^{n+1} - \mathbf{X}^n}{\Delta t} = \sum_{\mathbf{x}} \mathbf{u}^{n+1}(\mathbf{x})\,\delta_h^3(\mathbf{x} - \mathbf{X}^n(q,r,s))h^3. \tag{19}$$

In these equations time proceeds in steps of duration Δt, and superscripts denote the time-step index. Thus $\mathbf{u}^n(\mathbf{x}) = \mathbf{u}(\mathbf{x}, n\,\Delta t)$, and similarly for all other functions of time. The position variable $\mathbf{x}$ is restricted to a cubic lattice of points that has mesh width h in all three space directions. The notation $\Sigma_{\mathbf{x}}$ denotes the sum over this lattice. Similarly the fiber-point label (q,r,s) takes on only discrete values in which q is an integer multiple of Δq, r is an integer multiple of Δr, and s is an integer multiple of Δs. The notation $\Sigma_{q,r,s}$ denotes the sum over all these discrete fiber points. The parameters Δq, Δr, and Δs are all $O(h)$.

The partial difference operators appearing in Equations 9–19 are defined as follows. Given any function ϕ depending on any variable x, we define

$$(D_x^+\phi)(x) = \frac{\phi(x + \Delta x) - \phi(x)}{\Delta x}, \tag{20}$$

$$(D_x^-\phi)(x) = \frac{\phi(x) - \phi(x - \Delta x)}{\Delta x}, \tag{21}$$

$$(D_x^0\phi)(x) = \frac{\phi(x + \Delta x) - \phi(x - \Delta x)}{2\,\Delta x}. \tag{22}$$

In these equations, it is understood that all independent variables other than the named variable x are held constant. The vector difference operator $\mathbf{D}^0$ (corresponding to ∇) is defined as

$$\mathbf{D}^0 = \left(D_{x_1}^0, D_{x_2}^0, D_{x_3}^0\right). \tag{23}$$

It is used in Equations 17 and 18 to form the discrete gradient and divergence:

$$\mathbf{D}^0 p = \left(D_{x_1}^0 p, D_{x_2}^0 p, D_{x_3}^0 p\right), \tag{24}$$

$$\mathbf{D}^0 \cdot \mathbf{u} = D_{x_1}^0 u_1 + D_{x_2}^0 u_2 + D_{x_3}^0 u_3. \tag{25}$$

Note that Step 1 involves the explicit computation of the fiber force from the known fiber configuration at the beginning of the time step. This is the simplest possible approach and it is the one used to obtain the results in this paper. Note, however, that its use imposes a severe restriction on Δt to avoid numerical instability. For a more robust alternative, see Reference 3.

Step 3 is a statement of the projection method,[6,7] a fractional step method for the solution of the incompressible Navier–Stokes equations. The intermediate variables have been designated $\mathbf{u}^{n+1,i}$, where $i = 0, 1, 2, 3$. Equation 13 is essentially an explicit formula for $\mathbf{u}^{n+1,0}$. Equations 14, 15, and 16 are each a collection of tridiagonal systems for the unknowns $\mathbf{u}^{n+1,1}$, $\mathbf{u}^{n+1,2}$, and $\mathbf{u}^{n+1,3}$, respectively. Equations 17 and 18 are a pair of equations to be solved simultaneously for the unknowns $\mathbf{u}^{n+1}$ and p^{n+1}. (This is the projection step that gives the method its name.) The solution of Equations 17 and 18 may be found by using the fast Fourier transform.

III. THREE-DIMENSIONAL MODEL: RESULTS

The immersed boundary method was originally used to solve the equations of a two-dimensional model of the left heart only. Uses of that model have included studies concerning prolapse of the mitral valve,[8,9] optimal timing of atrial systole,[10] and improved design of prosthetic cardiac valves.[8,11–15] Here, we report the results of computations involving a three-dimensional model of the entire heart.

The model described here is anatomically complete. It includes left and right atria; left and right ventricles; the mitral, aortic, tricuspid, and pulmonic valves; superior and inferior vena cavae; four pulmonary veins; the ascending aorta; and the main pulmonary artery. The great vessels of the model have blind ends but are equipped with sources and sinks that can be used to connect the model heart to a simulated circulation. Another source–sink, located in the fluid external to the heart, establishes a reference pressure and accommodates the changes in volume that occur during the cardiac cycle.

All of the anatomical structures that we have just described are modeled as collections of elastic or contractile fibers (Plate 6*). The arrangement of these fibers in space is based on the principles of cardiac anatomy established by Thomas[16] and by Streeter et al.[17,18] Broadly speaking, the construction is done by choosing certain

* Plate 6 appears following page 49.

surfaces to represent the different layers of cardiac fibers and then laying out the fibers as geodesic curves on these surfaces.

A particularly interesting case is the model that we use for the aortic (and also for the pulmonic) valve.[19] Here, we have been able to derive the structure of the (closed) aortic valve from first principles, by solving the equations of equilibrium of a one-parameter family of fibers under tension supporting a uniform pressure load. These equations are

$$\frac{\partial}{\partial s}\left(T(r,s)\frac{\partial \mathbf{X}}{\partial s}\right) + p_0\left(\frac{\partial \mathbf{X}}{\partial s} \times \frac{\partial \mathbf{X}}{\partial r}\right) = 0, \tag{26}$$

where $\mathbf{X}(r, s)$ describes the fiber architecture of the closed aortic valve, with $r =$ constant designating a fiber and with $s =$ arc length along a fiber. (For each leaflet, we set $s = 0$ in its plane of symmetry, which is orthogonal to the fibers, and we set $r = 0$ along the free leaflet margins.) The function $T(r, s)$ is the fiber tension in the sense that $T(r, s)\,dr$ is the force transmitted by the strip of fibers $(r, r + dr)$. The direction of this force is the unit tangent to the fibers $\partial \mathbf{X}/\partial s$, which is a unit vector because $s =$ arc length. The constant p_0 is the uniform pressure applied to the closed aortic valve by the blood. Equation 26 has the following consequences:

1. The tension is constant along each fiber: $T = T(r)$, independent of s.
2. The fibers are geodesics on the leaflet surface.
3. The fibers ($r =$ constant) and the curves $s =$ constant form an orthogonal net on the leaflet surface. (To derive this, we need the fact that the curve $s = 0$ is orthogonal to the fibers.)

By an appropriate choice of the parameter r, we may eliminate the mechanical variables T and p_0 and derive a purely geometric equation,

$$\frac{\partial \mathbf{X}}{\partial r} = \frac{\partial \mathbf{X}}{\partial s} \times \frac{\partial^2 \mathbf{X}}{\partial s^2}, \tag{27}$$

which, together with suitable boundary conditions,[19] determines the shape of the leaflet and the arrangement of its fibers. Equation 27 may be solved numerically by a method developed by Buttke[20] for the study of vortex motion in superfluid turbulence.

The resulting valve has astonishing complexity (see Plate 7*), which may be traced to a singularity that necessarily exists at the center of the valve, where the three leaflets meet. Similar complexity is observed in the structure of real aortic leaflets stained for collagen.[21] A challenge for the future is to carry out a similar program for the heart as a whole, i.e., to derive the fiber architecture of the heart from first principles. For progress in this direction, see Reference 22.

The three-dimensional model heart is shown in action in Plate 8,* and a close-up of the model aortic valve in action is shown in Plate 9.* In these plates, fluid motion is depicted in terms of streak lines, with a blob at the current position of a fluid marker and a tail showing its recent trajectory.

* Plates 7 to 9 appear following page 49.

IV. SUMMARY AND CONCLUSIONS

In summary, we have devised a computational method for determining the flow of a viscous incompressible fluid in the presence of flexible boundaries with which the fluid interacts, and we have applied that method to the study of blood flow in a three-dimensional model of the heart.

Further research is needed in the following areas:

1. Adjustment of the anatomy and physiology of the model heart to make it more realistic,
2. Parallel implementation of the immersed boundary method to improve turnaround time,
3. Modification of the immersed boundary method itself to allow for Reynolds numbers within the physiological range,
4. Development of a mathematical theory from which the fiber architecture of the heart can be derived.

Applications of this work include the investigation of normal cardiac function, the simulation of disease processes affecting the mechanical function of the heart or its valves, and the computer-assisted design of prosthetic cardiac valves.

ACKNOWLEDGMENTS

This research was supported in part by the National Institutes of Health under Research Grant HL17859 and under the Biomedical Computing Initiative at the Pittsburgh Supercomputing Center. Support was also provided by the National Science Foundation through the Geometry Center, University of Minnesota. Computations were performed on the Cray Y-MP at the Pittsburgh Supercomputing Center and on the Cray-2 at the National Center for Supercomputing Applications, University of Illinois. Computer-generated graphics were created at New York University on IRIS workstations of the ACF Visualization Center and the Geometry Center, using software written by one of the authors (D. M. M.). We thank A. A. H. J. Sauren for permission to reproduce Plate 7c.

REFERENCES

1. Peskin, C. S., Flow Patterns Around Heart Valves: A Digital Computer Method for Solving the Equations of Motion, Ph.D. thesis, Albert Einstein College of Medicine, 1972 (available from University Microfilms, 72-30, 378).
2. Peskin, C. S., Numerical analysis of blood flow in the heart, *J. Comput. Phys.*, 25, 220–252, 1977.
3. Peskin, C. S. and McQueen, D. M., A three-dimensional computational method for blood flow in the heart. I. Immersed elastic fibers in a viscous incompressible fluid, *J. Comput. Phys.*, 81, 372–405, 1989.
4. McQueen, D. M. and Peskin, C. S., A three-dimensional computational method for blood flow in the heart. II. Contractile fibers, *J. Comput. Phys.*, 82, 289–297, 1989.
5. Peskin, C. S. and McQueen, D. M., Computational biofluid dynamics, *Contemp. Math.*, in press, 1992.
6. Chorin, A. J., Numerical solution of the Navier–Stokes equations, *Math. Comp.*, 22, 745–762, 1968.
7. Chorin, A. J., On the convergence of discrete approximations to the Navier–Stokes equations, *Math. Comp.*, 23, 341–353, 1969.
8. McQueen, D. M., Peskin, C. S., and Yellin, E. L., Fluid dynamics of the mitral valve: Physiological aspects of a mathematical model, *Am. J. Physiol.*, 242, H1095–H1110, 1982.

9. Printz, B. F., Peskin, C. S., Yellin, E. L., and Teichholz, L. E., Effects of mitral apparatus geometry on mitral flow and leaflet motion: A computer study, *J. Am. Coll. Cardiol.*, submitted.
10. Meisner, J. S., McQueen, D. M., Ishida, Y., Vetter, H. O., Bortolotti, U., Strom, J. A., Frater, R. W. M., Peskin, C. S., and Yellin, E. L., Effects of timing of atrial systole on LV filling and mitral valve closure: Computer and dog studies, *Am. J. Physiol.*, 249, H604–H619, 1985.
11. Peskin, C. S. and McQueen, D. M., Modeling prosthetic heart valves for numerical analysis of blood flow in the heart, *J. Comput. Phys.*, 37, 113–132, 1980.
12. McQueen, D. M. and Peskin, C. S., Computer-assisted design of pivoting-disc prosthetic mitral valves, *J. Thoracic Cardiovasc. Surg.*, 86, 126–135, 1983.
13. McQueen, D. M. and Peskin, C. S., Computer-assisted design of butterfly bileaflet valves for the mitral position, *Scand. J. Thoracic Cardiovasc. Surg.*, 19, 139–148, 1985.
14. McQueen, D. M. and Peskin, C. S., Curved butterfly bileaflet prosthetic cardiac valve, U.S. Patent Number 5026391, 1991.
15. McQueen, D. M. and Peskin, C. S., A heart valve prothesis, European Patent Publication Number EP 0 211 576 B1, 1990.
16. Thomas, C. E., The muscular architecture of the ventricles of hog and dog hearts, *Am. J. Anatomy*, 101, 17–57, 1957.
17. Streeter, D. D., Jr., Spotnitz, H. M., Patel, D. P., Ross, J., Jr., and Sonnenblick, E. H., Fiber orientation in the canine left ventricle during diastole and systole, *Circ. Res.*, 24, 339–347, 1969.
18. Streeter, D. D., Jr., Powers, W. E., Ross, M. A., and Torrent-Guasp, F., Three-dimensional fiber orientation in the mammalian left ventricle wall, in *Cardiovascular System Dynamics*, Baan, J., Noordergraaf, A., and Raines, J., Eds., MIT Press, Cambridge, MA, 1978, pp. 73–84.
19. Peskin, C. S. and McQueen, D. M., Mechanical equilibrium determines the fractal fiber architecture of the aortic heart valve leaflets, *Am. J. Physiol.*, submitted.
20. Buttke, T. F., A numerical study of superfluid turbulence in the self-induction approximation, *J. Comput. Phys.*, 76, 301–326, 1988.
21. Sauren, A. A. H. J., The Mechanical Behavior of the Aortic Valve, Ph.D. thesis, Eindhoven Technical University, The Netherlands, 1981.
22. Peskin, C. S., Fiber architecture of the left ventricular wall: An asymptotic analysis, *Commun. Pure Appl. Math.*, 42, 79–113, 1989.